Kinematics of densely flowing granular mixtures

K. M. Hill
St. Anthony Falls Laboratory, Department of Civil Engineering, University of Minnesota, Minneapolis, Minnesota 55414, USA

J. Zhang
Theoretical and Applied Mechanics, University of Illinois, Urbana, Illinois 61801, USA

(Received 24 December 2007; revised manuscript received 12 April 2008; published 12 June 2008)

We measure the kinematics of segregating granular mixtures in dense free-surface boundary-layer flow in a rotated drum. We find that in a segregating mixture, the different components move with roughly the same velocities, except for a relatively small segregation velocity perpendicular to the direction of flow. On the other hand, the mean variance of the velocities—often associated with a *granular temperature*—may differ for the two components. In the majority of the high-density boundary layer, the difference is driven by relative particle size and may be understood considering a geometrically motivated model. In the low-density region at the top of the boundary layer, the difference is driven by relative particle mass, similar to observations in more energetic systems.

DOI: 10.1103/PhysRevE.77.061303 PACS number(s): 45.70.−n, 47.57.Gc

I. INTRODUCTION

Mixtures of macroscopic particles appear uncomplicated by their very nature; the particles interact only through apparently simple contact forces [1]. Yet the bulk material response to external excitation is often difficult to predict. Notably, the local interactions often result in system-spanning segregation patterns whose details are sensitive to subtle changes in particle properties. For example, when particulate mixtures are poured into a box, the components may segregate either along the direction of the flow only or, additionally, into stratified layers. The difference arises in part from the frictional properties of the particles [2]. Alternatively, when rotated in circular drums, most mixtures tend to segregate into circularly symmetric patterns, but when the particles differ in size, they may segregate into radial stripes [3,4] (Fig. 1).

To this point, there has been no causal relationship found between the particle properties (e.g., size, density) and the kinematics of bulk behavior (e.g., velocity, velocity variance) that might give rise to the difference in the segregation patterns. Such a link could aid in the development of a continuum model that has predictive power for segregation behaviors in these systems.

There have been some detailed studies on the dynamics of components in more sparse and energetic granular mixtures. Specifically, Garzó and Dufty [5] investigated the cooling process of a granular mixture using Enskog kinetic theory and found that the components may have different *granular temperatures*—analogous to the kinetic energy of the velocity variances. They found that the ratio of the granular temperatures of the components depended on the relative particle mass, relative number density, and restitution coefficient. Other experimental and computational research has verified what is called by some this "energy equipartition breakdown" for a variety of mixtures [6–9]. The details of how the relative *granular temperature* depends on system parameters varies from one system to the next. In all cases, the granular temperature ratio appears inversely related to particle mass (size and density). Some theoretical and computational studies point toward an additional dependence on the restitution coefficient and relative particle number density [5–7]. Feitosa and Menon [8] studied the problem experimentally for mixtures differing only in density and found no dependence on the restitution coefficient or number density—i.e., that the variability in their systems depended only on mass (i.e., material density). Wildman and Parker [9] investigated this question for mixtures differing only in size and found a dependence of relative granular temperatures both on the relative mass (i.e., in this case, size) and on the relative number density of the components.

Here, we investigate how the particle properties of components in a *dense gravity-driven* granular mixture affect the

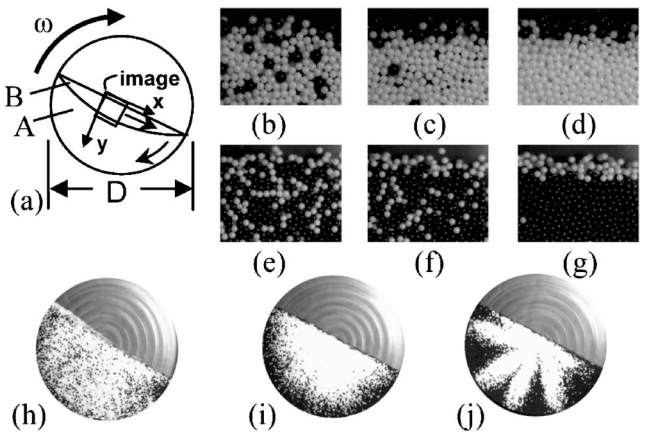

FIG. 1. (a) A sketch of the experiment, a rotating drum halfway filled with beads. At any time, most beads rotate with the drum (a) while a thin layer (b) slides quickly over the rest. (b)–(g) Images taken as indicated in (a) of (b)–(d) 3-mm (dark) and 2-mm (light) plastic beads; (e)–(g) 2-mm steel (dark) and plastic (light) beads, first mixed, then rotated in a drum after (b),(e) 1/4 rot; (c),(f) 3/4 rot; and (d),(g) ≈10 rot. (h),(i) Pictures of the whole drum (h) before and (i) after segregation typical of mixtures rotated slowly in a half-filled drum. (j) An image of the steady segregation pattern with the drum filled ~55% with a mixture of 2- and 3-mm plastic beads.

kinematic behaviors of the particles relative to those of the mixture. Experimentally, we query how the type of particulate mixture (different density versus different size) affects the kinematics of dense free-surface boundary-layer flow through experimental measurements of two differently segregating mixtures in a rotated drum. We find the most noteworthy differences appear not in the segregation velocities, but in the average variance of the velocities of the components in the mixture. In contrast to the results from more energetic mixtures described above, this difference appears driven by size alone in most of the boundary layer. Specifically, particles smaller than other components in the mixture have a higher mean velocity variance than their neighboring larger counterparts; particles in mixtures that differ only in density have similar velocity variances to their neighbors of different density. We further test this computationally for mixtures varying in both size and density, and the dependence of the relative velocity variance on relative particle size (not density) appears to hold.

In contrast, for a very narrow low-density region at the top of the flowing layer, we find that the velocity variance differences depend on relative mass (dependent on both size and density) of the particles, similar to results in energetic sparse mixtures described above [5–9].

II. EXPERIMENTS

We experimentally study two types of mixtures: one where the particles differ only in density (plastic and steel beads all of diameter $d=2$ mm), the other where the particles differ only in size (plastic beads whose diameters are $d=2$ and 3 mm) [10]. The contribution of each component to the mixture by volume (V_i) is varied according to the following: $V_1:V_2=100:0$, 75:25, 50:50, 25:75, and 0:100. The results for single-component systems have been presented in detail in previous articles (Refs. [11,12]), so here we primarily discuss them qualitatively for comparison with our most recent mixture results.

We fill a thin transparent circular drum (diameter $D \approx 300$ mm, thickness $t \approx 8$ mm, material, acrylic) halfway with these mixtures. We rotate the drum at $\omega \approx 1$ rpm, which generates a thin flat flowing layer that is relatively uniform in the x direction [see Fig. 1(a)] in the center of the drum. While the drum rotates, we focus a high-resolution digital camera on this region of the flowing layer, and once every half rotation, we take 1024 images at 500 fps. We begin this routine after $\approx \frac{1}{4}$ rotation to avoid transients associated with the initial flow of the particles in the drum. We repeat at intervals of $\frac{1}{2}$ rotation subsequently. All results shown represent the average of three sets of such experiments.

We begin the rotation when the beads are well mixed. During the first half rotation of the drum, all beads enter the flowing layer well mixed, as in Figs. 1(b), 1(e), and 1(h). As commonly observed, the components quickly segregate—the smaller (or alternatively, denser) beads sink in the flowing layer, apparently in less than 1 rotation, Figs. 1(c), 1(f), and 1(i). At the fill level used (50%), the subsequent change is limited to a further sharpening of the boundary between the segregating components [13]. The segregation patterns in the

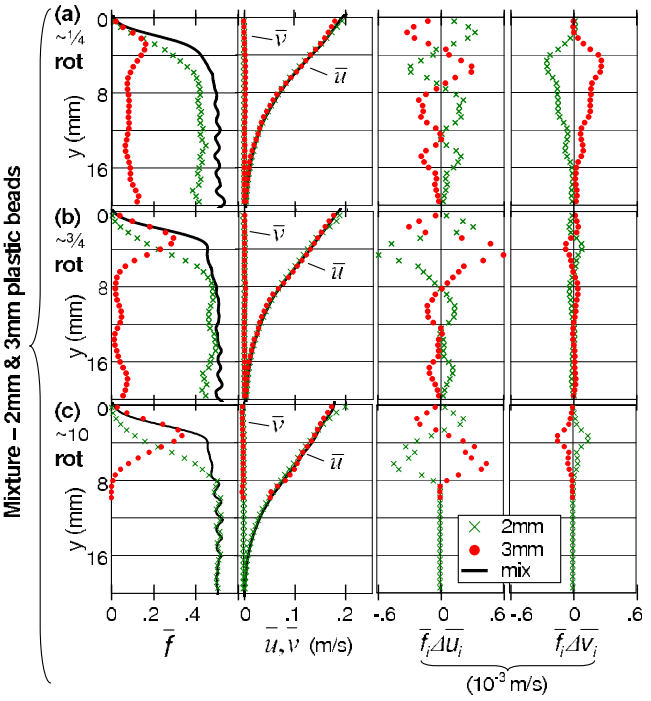

FIG. 2. (Color online) Experimental results for the 50:50 mixture of 2- and 3-mm plastic beads shown in Figs. 1(b)–1(d). (a) $\bar{f}$, $\bar{u}$, $\bar{f}_i \Delta \bar{u}_i$, and $\bar{f}_i \Delta \bar{v}_i$ for the mixed state—i.e., for $\sim 1/4$ rot of the drum. (b) The same after $\sim 3/4$ rot of the drum. (c) The same, ~ 10 rot, where the system is in a steady state [27].

systems described in this paper reach a steady state after two to three rotations, with a relatively constant fraction of larger (or, alternatively, less dense) beads on the top of the flowing layer [Figs. 1(d) and 1(g)].

For each experiment (i.e., each set of 1024 images), we locate and track the beads from one image to the next. From this, we calculate the mean volume fraction $\bar{f}(y)$ for each component and for the mixture, as well as the mean velocities and velocity variances (velocity fluctuation correlations) $\bar{u}(y)$, $\bar{v}(y)$, $\overline{u'u'}(y)$, $\overline{v'v'}(y)$, and $\overline{u'v'}(y)$ [14]. (Here and henceforth, $\bar{*}$ refers to the quantity $*$ averaged both in the x direction and over the duration of a single set of images.) Here, u and v are the instantaneous velocities parallel and perpendicular to the average flow, $u'=u-\bar{u}$ and $v'=v-\bar{v}$, where, in terms of the component directions shown in Fig. 1(a), the velocity $\vec{v}=u\hat{\mathbf{x}}-v\hat{\mathbf{y}}$. We also calculate the flux of each component relative to the mixture, parallel and perpendicular to the average flow: $\bar{f}_i \Delta \bar{u}_i = \bar{f}_i(\bar{u}_i - \bar{u}_{mix})$ and $\bar{f}_i \Delta \bar{v}_i = \bar{f}_i(\bar{v}_i - \bar{v}_{mix})$. Figure 2 shows the volume fractions, velocities, and fluxes for the 50:50 mixture of 2- and 3-mm plastic beads—"before" [Fig. 2(a)], "during" [Fig. 2(b)], and "after" [Fig. 2(c)] segregation.

The results for the mixed phase (solid lines in the plots) are qualitatively similar to results for monodisperse systems [11,12,15]: $\bar{f}_{mix}$ is low near the free surface and increases quickly to 50% within 4–6 mm ($\sim 2\bar{d}$, where $\bar{d}$ is the locally averaged particle size); $\bar{u}_{mix}$ is highest near the free surface and decreases to zero within $5\bar{d}-6\bar{d}$. The plots of $\bar{f}_i$ for the

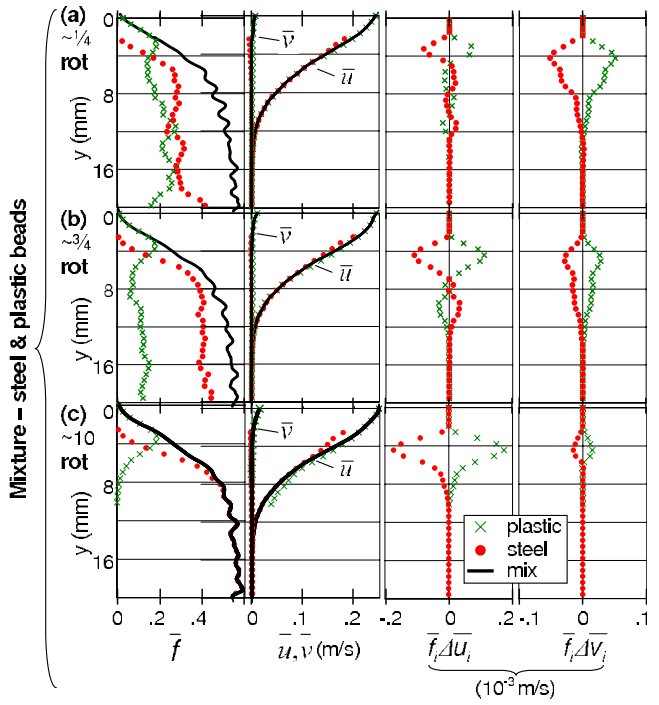

FIG. 3. (Color online) Experimental results for the 50:50 mixture of 2-mm plastic and 2-mm steel beads shown in Figs. 1(e)–1(g). (a) $\bar{f}$, $\bar{u}$, $\bar{f}_i\Delta\bar{u}_i$, and $\bar{f}_i\Delta\bar{v}_i$ for the mixed state—i.e., for ~1/4 rot of the drum. $\Delta\bar{u}_i=\bar{u}_i-\bar{u}_{mix}$ and $\Delta\bar{v}_i=\bar{v}_i-\bar{v}_{mix}$, where i refers to each component. (b) The same after ~3/4 rot of the drum. (c) The same, ~10 rot, where the system is in a steady state.

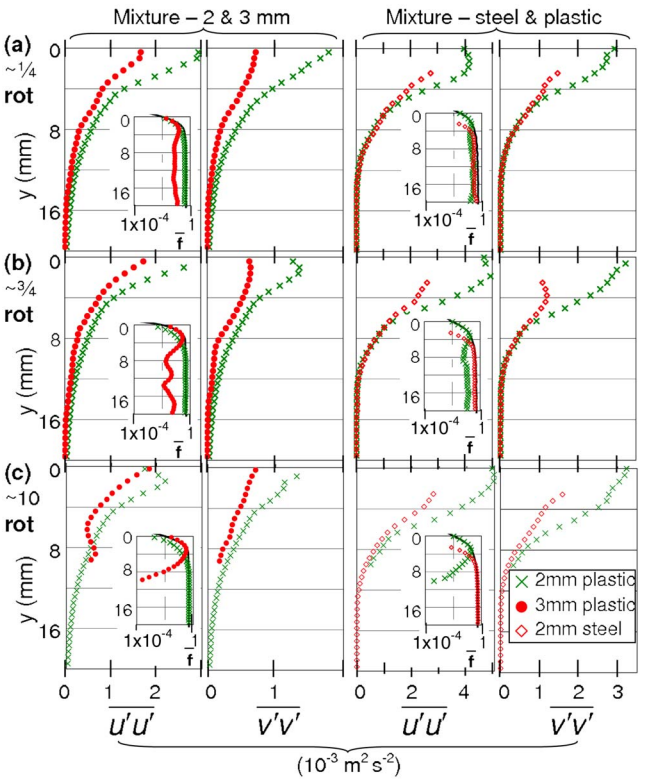

FIG. 4. (Color online) (a) $\overline{u'u'}(y)$ and $\overline{v'v'}(y)$ for the 50:50 mixture of 2- and 3-mm plastic beads (first two columns) and the 50:50 mixture of 2-mm plastic and steel beads (last two columns). Results for the mixed state—i.e., for ~1/4 rot of the drum. (b) The same after ~3/4 rot of the drum. (c) The same, ~10 rot, where the system is in a steady state. The insets show the volume fraction $\bar{f}$ for the mixed state and the individual components on linear-log plots, showing that after 10 rot, for $y>8$ mm, the volume fraction of the particles that segregate upwards (the 3-mm particles in the first two columns and the plastic particles in the second two columns) falls below 1%, representative of less than a single bead.

individual components (distinct symbols in the plots) reflect the segregation apparent by eye. (The volume fraction of large beads seems disproportionately low due to the presence of the wall; we discuss this shortly.) Both $\bar{u}_i$ and $\bar{v}_i$ are similar for both components at any given depth, though not identical, as is more apparent in the plots for the flux $(\bar{f}_i\Delta\bar{u}_i,\bar{f}_i\Delta\bar{v}_i)$. Initially, the smaller beads *sink* (with gravity) perpendicular to the free surface, relative to the mixture, and the larger beads *rise*. This difference vanishes quickly corresponding to the quick segregation [Fig. 1(b) and 1(c)]. In contrast, the fluxes parallel to the flowing layer $(\bar{f}_i\Delta\bar{u}_i)$ show no trend for the mixed state, though after segregation, the large beads drift forward relative to small beads at the same depth, except at the free surface (where $\bar{f}_{mix}<40\%$).

Many of these details are similar for particulate mixtures where the components differ in density only (Fig. 3): $\bar{f}_{mix}$ is low near the free surface and increases quickly to 50%, though a bit farther from the free surface than for the 2- and 3-mm bead mixture. This extended low-density region is most likely a result of two factors: First, the large difference in particle mass means that collisions between the plastic and steel beads near the surface can result in a projection of the lighter (plastic) beads out of the bulk. Second, (compared to a similar effect for the steel beads) the small ratio between the weight of the plastic beads and air friction acting on these beads once aloft slows the beads as they fall enough to maintain a relatively consistent sparse layer from settling to the denser region below. As is the case for the 2- and 3-mm mixture, $\bar{u}_{mix}$ is highest near the free surface and decreases to zero within $5d-6d$. In the plots of the individual components, there are other similarities. Initially, the denser beads *sink* (with gravity) perpendicular to the free surface, relative to the mixture, and the less dense beads *rise*. Also, the measurements for $\bar{f}_i\Delta\bar{u}_i$ are similar for both components for the mixed state, and after segregation, the less dense beads drift forward relative to the denser particles. In summary, for these two types of mixtures, there are no qualitative differences between mean velocities and velocity fluxes for the components relative to the mixture.

On the other hand, the behaviors of the mean velocity *variances* $\overline{u_i'u_i'}(y)$ and $\overline{v_i'v_i'}(y)$ do qualitatively differ from one type of mixture to the next (see Fig. 4). In the mixtures of 2- and 3-mm beads, the mean variance of the velocities of the smaller beads are greater than those of the larger particles at any given depth. In contrast, the relative variance of the plastic and steel beads depends on the region of the flowing layer. Near the top, where the flow is energetic and sparse, $\overline{u_i'u_i'}(y)$ and $\overline{v_i'v_i'}(y)$ are greater for the plastic beads than for the steel beads. Lower in the layer, where $\bar{f}_{mix}>0.4$ and

beads are in enduring contact with neighboring particles, $\overline{u_i'u_i'}(y)$ and $\overline{v_i'v_i'}(y)$ are nearly the same for the steel and plastic beads. A possible exception to this rule is apparent for deep regions, $y>8$ mm, after segregation—i.e., in Fig. 4(c) where the concentration of particles that rise over the course of the experiment is quite low [$\bar{f}_{3\mathrm{mm}}$ in column 1 and $\bar{f}_{plastic}$ in column 3 of Fig. 4(c), included as linear-log plots in the insets]. Where the volume fractions and the speeds are this low, the results are representative of only a fraction of a single particle. We include these points for completeness, though we believe they are statistically insignificant and do not affect our conclusions from these experiments: specifically, that the relative velocity variances of the components in a densely flowing granular mixture depend only on relative size and not relative density.

In the dense part of the flow, the dependence of the velocity variances $\overline{u_i'u_i'}(y)$ and $\overline{v_i'v_i'}(y)$ only on the size of the particles relative to the mixture is likely due to geometric constraints related to the nature of the flow, as described in Ref. [12] for monodisperse systems. The essence of this model is as follows. Particle movement in this dense flow is primarily laminar in nature, where particles move in enduring contact over neighboring layers of particles below them. Velocity fluctuations are generated when beads must slide around neighbors below or when the neighbors below push them as they themselves slide around their neighbors. We can extend this qualitatively to particles of different properties by noting that particles sliding over larger neighbors will be jostled more than particles sliding over smaller particles.

Following the arguments in Ref. [12], we can model the velocity fluctuations as sinusoidal variations in the velocity of a relative frequency of $\bar{u}_{rel}/\bar{d}$ and an amplitude that scales as $\bar{u}_{rel}$, the average velocity of a layer of particles relative to the neighboring layer below. Specifically, $u_{rel,i}=\bar{u}_{rel}+\bar{u}_{rel}\xi_{u,i}\cos[(\bar{u}_{rel}/\bar{d})t]$ and $v_{rel,i}=\bar{u}_{rel}\xi_{v,i}\cos[(\bar{u}_{rel}/\bar{d})t-\phi_i]$, where $\xi_{u,i}$ and $\xi_{v,i}$ are proportionality constants and ϕ_i is the phase difference between the "jostling" in each direction. Following this model (see [12] for details) the velocity fluctuation correlations (i.e., the mean velocity variances) may be written $\overline{v_i'v_i'}(y)=\frac{\xi_{v,i}^2}{2}\int_y^{y_b}\bar{d}(\eta)\dot{\gamma}^2(\eta)d\eta$ and $\overline{u_i'u_i'}(y)=\frac{\xi_{u,i}^2}{2}\int_y^{y_b}\bar{d}(\eta)\dot{\gamma}^2(\eta)d\eta$ and the cross correlation $\overline{u_i'v_i'}(y)=\xi_{u,i}\xi_{v,i}\frac{\cos\phi_i}{2}\int_y^{y_b}\bar{d}(\eta)\dot{\gamma}^2(\eta)d\eta$. Here, y_b is the depth at the bottom of the flowing layer, $\dot{\gamma}(\eta)=d\bar{u}/d\eta$, and $\bar{d}(\eta)$ is the average diameter at depth $y=\eta$. When this model is fit to the data for these mixtures, the results are in reasonable agreement for the bulk dense granular flow, as shown in Fig. 5. However, there is a narrow region at the top where the fit works less well. This point at which the quality of the fit degrades appears to correspond to a depth at which there is a change in the slope of $\bar{f}$, approximately for $\bar{f}<0.4$ (see Fig. 2). This is approximately the same critical value of $\bar{f}$ for the plastic and steel beads: where $\bar{f}>0.4$, $\overline{u'u'}(y)$ and $\overline{v'v'}(y)$ are approximately the same for the two components and where $\bar{f}<0.4$, $\overline{u'u'}(y)$ and $\overline{v'v'}(y)$ for the two components diverge.

One explanation for this apparent change in behavior follows similar arguments as those posed in Refs. [11] and [12]:

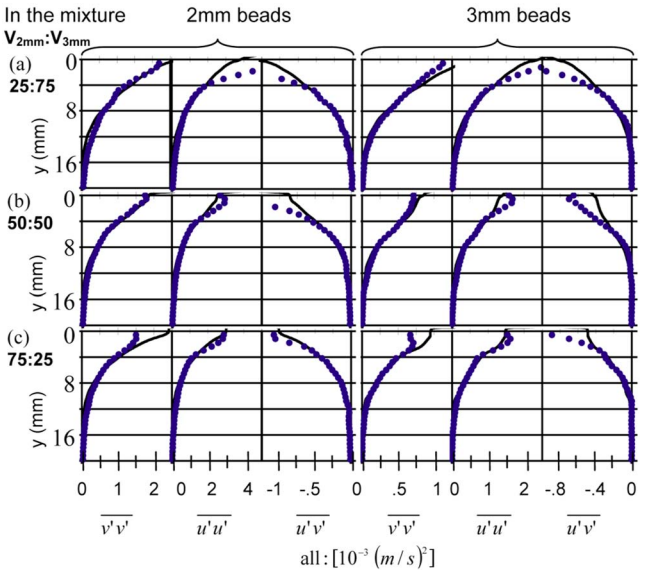

FIG. 5. (Color online) Fits of the geometric model described in the text (solid lines) to the experimental data (points) for the (a) 25:75, (b) 50:50, and (c) 75:25 2- and 3-mm plastic bead mixture. The solid circles are measured data points, and the lines are the model fits. The first three columns show data and fits for the 2-mm beads in the mixture; the latter three columns show data and fits for the 3-mm beads in the mixture. The fitting parameters [ξ_v,ξ_u,ϕ (rad)] are (a) 2 mm (1.0,0.9,1.8), 3 mm (0.8,0.7,1.8); (b) 2 mm (1.0,0.8,1.8), 3 mm (0.8,0.6,1.8); (c) 2 mm (0.9,0.8,1.8), 3 mm (0.7,0.6,1.8). For the 2-mm plastic and steel bead mixture, the results (not shown) are nearly the same for all beads for all percentages: $(\xi_v,\xi_u,\phi)\sim(1.0,0.8,1.8)$.

there are two types of flow within this free-surface boundary layer, one of dense laminar flow of enduring interparticle contacts and a more energetic, sparse region where collisions are more important for determining kinematic and kinetic details. In the less dense region where particle-particle contacts are not enduring and collisions become more important than sliding contacts in momentum transfer, mass (rather than size or density) should dominate the behavior of the velocity fluctuations. To investigate this transition, we use computational simulations so that both size and density may be smoothly varied and the effect of mass isolated.

III. COMPUTATIONAL SIMULATIONS

To study these systems computationally, we use the discrete (or distinct) element method (DEM), first proposed by Cundall and Strack [16], whereby motions of every discrete solid particle are tracked and a simple "soft sphere" force law is used to describe particle-particle interactions. We use the nonlinear force model that incorporates Hertzian contact theory and material properties into the contact coefficients by Tsuji *et al.* [17].

First, to understand the impact of the sidewall on the details described above, we examine results from a simulated 50:50 mixture of 2- and 3-mm particles rotated in a drum (Fig. 6). The drum size is smaller than the physical experiments (here $D=72$ mm) to reduce the computational time.

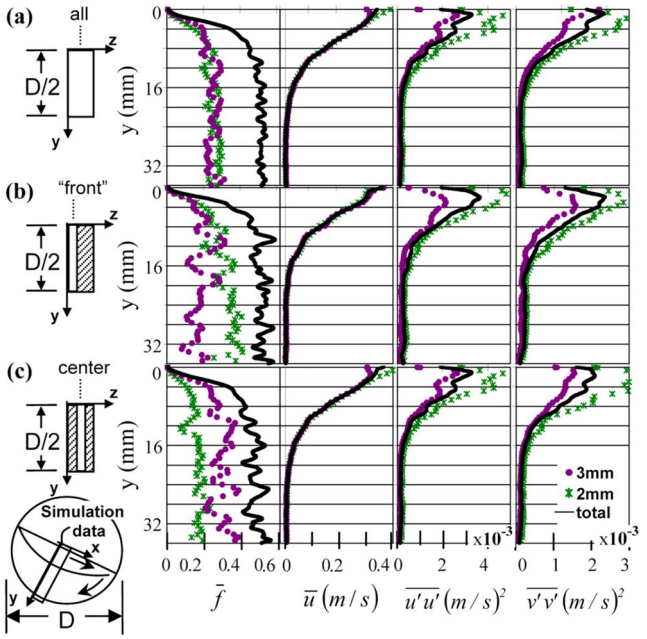

FIG. 6. (Color online) Simulation results for a mixture of 2- and 3-mm beads rotated in a $D=72$ mm, $t\sim 8$ mm drum at $\omega=16$ rpm after $\sim 1/4$ rot [compare with Fig. 2(a)]. Results for (a) the entire width of the mixer, (b) the front third of the mixer (most comparable to experimental results), and (c) the middle third of the mixer. The data included are indicated in the sketch at the bottom of Fig. 6.

Accordingly, the rotational velocity is increased according to scaling laws proposed by Taberlet *et al.* [18] so that $\omega \approx 16$ rpm. These results show that the larger particles are crowded away from the sidewalls; that is, small particles tend to be more highly concentrated against the side walls, while larger particles are more highly concentrated in the gap away from the sidewalls. This explains the disproportionately low volume fraction of 3-mm particles in Figs. 2(a)–2(c) [19]. Nevertheless, the same trends in $\bar{u}(y)$, $\overline{u'u'}(y)$, and $\overline{v'v'}(y)$ occur throughout the drum for both components and the mixture, as might be expected for such a narrow drum.

Next, we use the computational simulations to determine how the velocity fluctuations depend on the mass, independent of size, by varying the density of the particles relative to one another. We use the same computational drum, but with periodic boundaries rather than sidewalls, so that the anomalous sidewall effects described above do not arise. We use beads of 2 and 3 mm and vary the mass ratio $M_r=M_3/M_2$ from ≈ 0.8 to 5.5.

Figure 7 shows $\overline{u_i'u_i'}(y)$ and $\overline{v_i'v_i'}(y)$ for four values of M_r: from $M_r\approx 0.8$ [Fig. 7(a)] to $M_r\approx 2.7$ [Fig. 7(d)]. The insets show $f_i(y)$ and $f_{mix}(y)$ for each case. Notably, at approximately 5 mm below the free surface f_{mix} abruptly changes slope as it nears its maximum value of approximately 0.6 [20]. Below a depth of 4–5 mm, $\overline{u_i'u_i'}(y)$ and $\overline{v_i'v_i'}(y)$ appear independent of M_r and the values of $\overline{u_i'u_i'}(y)$ and $\overline{v_i'v_i'}(y)$ for small particles are greater than those for larger particles. Closer to the free surface where the flow is less packed, the relative values of $\overline{u_i'u_i'}(y)$ and $\overline{v_i'v_i'}(y)$ clearly vary with M_r.

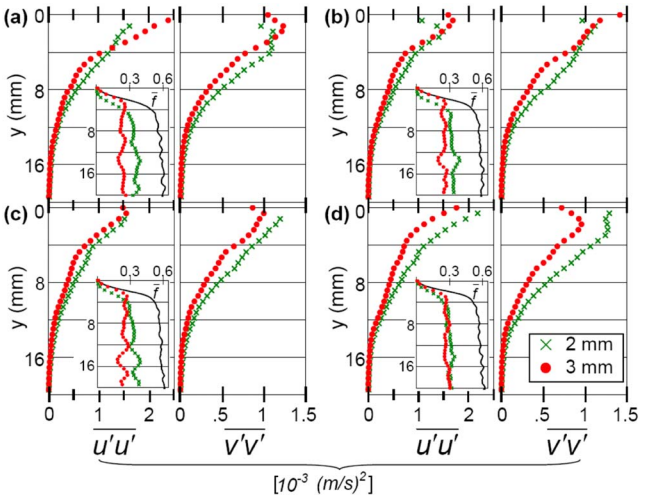

FIG. 7. (Color online) Simulation results for velocity variances of a mixture of 2- and 3-mm beads rotated $\sim 1/4$ rot. (a) $M_r\sim 0.8$, (b) $M_r\sim 1$, (c) $M_r\sim 1.73$, and (d) $M_r\sim 2.74$.

In this region, the magnitudes of $\overline{u_i'u_i'}(y)$ and $\overline{v_i'v_i'}(y)$ are greater for the lighter particles than the heavier particles, and for $M_r=1$ [Fig. 7(b)], $\overline{u_i'u_i'}(y)$ and $\overline{v_i'v_i'}(y)$ are approximately equal for the two components.

To investigate this further, we sum $\overline{u_i'u_i'}(y)$ and $\overline{v_i'v_i'}(y)$ for each species i—one might call this the *kinematic temperature* $T_{kinem,i}=\overline{u_i'u_i'}(y)+\overline{v_i'v_i'}(y)$. Then we calculate the ratio of $T_{kinem,i}$ for the two components for each mixture: $T_{kinem,r}=T_{kinem,3}/T_{kinem,2}$. The results are graphed in Fig. 8.

In the graph and inset in Fig. 8(a), two distinct regions are evident. Below a depth of approximately 5 mm, $T_{kinem,r}$ is roughly independent of both the mass ratio of the particles and the depth. This further supports the form of the geometric model described in the experiment section. With a bit of algebra [21] one might show that the model predicts $T_{kinem,r}=(\xi_{u,3}^2+\xi_{v,3}^2)/(\xi_{u,2}^2+\xi_{v,2}^2)$, independent of depth. The results shown in Fig. 5 indicate that this value should be approximately 0.7, similar to that found for $\bar{f}>0.4$ in these simulations.

On the other hand, where the volume fraction is relatively low ($y<5$ mm)—that is, where particles are no longer in

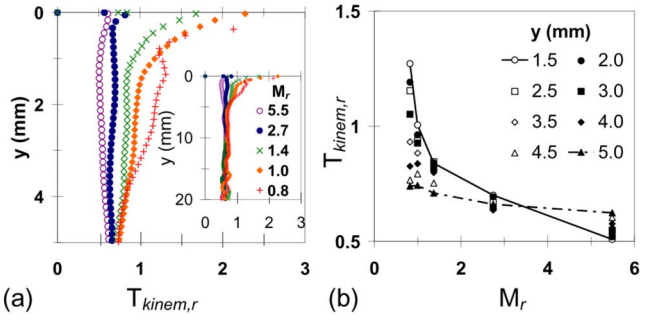

FIG. 8. (Color online) Kinematic temperature ratio for mixtures of 2- and 3-mm beads of varying mass ratios as indicated in the plots. (a) The dependence of the temperature ratios on depths for the five mixtures as indicated. (b) The dependence of the temperature ratio on the mass ratios for distinct depths as indicated in the legend.

enduring contact and collisions are more important for momentum transfer—$T_{kinem,r}$ is inversely related to M_r (and ρ_r). In fact, for a narrow range of depths (1.5 mm$<y<$3 mm) corresponding to $0.1<\bar{f}<0.4$ the results for T_r correspond to what one might expect from simple momentum conservation arguments: for $M_r=1$, $T_{kinem,r}\approx 1$; for $M_r<1$, $T_{kinem,r}>1$; and for $M_r>1$, $T_{kinem,r}<1$. The results in this region are analogous to those obtained by Feitosa and Menon [22] for more uniform shaken systems.

In summary, the relative mean velocities and fluxes of the components of the different mixtures behave similarly. During segregation one species sinks in the direction perpendicular to the average flow. *This* "sinking" has been explained through mechanisms such as buoyancy [23] for particles that differ in density and kinetic sieving [24] for particles that differ in size and is directly related to the observed radial segregation in all systems, independent of mixture. After this segregation has stabilized, the same species that sinks perpendicular to the flow drifts backward parallel to the flow. This has not been previously reported, although it also appears to be common for all mixtures investigated. On the other hand, the mean velocity variances of particle components behave differently. The differences depend on how the component properties compare with other components in the mixture and also on the state of flow and associated interparticle interactions. In the dense region of flow, the variances, or velocity fluctuations, scale (inversely) only with size, *not* with density. In contrast, in the less dense region, they scale (inversely) with mass (size and density). This result is similar to those observed in more energetic systems, although there are additional effects reported such as that due to the coefficient of restitution and volume fraction effects that were not investigated in the research reported here [5–9].

While not entirely intuitive, the difference in velocity fluctuations in dense granular flow may be a first step toward understanding the segregation differences in densely flowing granular mixtures. The velocity fluctuations might quantify an apparent fluidity difference mentioned by Jain *et al.* [4] and subsequent system-scale segregation patterns. Galvin *et al.* [6] demonstrated that in certain granular mixtures a difference in mean velocity fluctuations or variances manifests itself as a *segregation force*.

Developing a predictive model for segregation behaviors as they depend on different particle properties is important for many natural applications. For example, in riverbeds the formation and maintenance of gravel patches of relatively uniform-sized particles suitable for fish habitat are among important considerations for river restoration problems [25]. A significant annual expense for some river restoration projects lies in gravel augmentation—and understanding of the behavior of gravel as a function of its size may improve the longevity and reduce the expense of these projects. In debris flows, the largest boulders tend to gather toward the front and likely are responsible for the most wear and damage [26]. A better understanding and improved modeling of the behavior of granular mixtures as they depend on their components may aid in both environmental restoration and disaster mitigation.

ACKNOWLEDGMENTS

The authors gratefully acknowledge the assistance of V. Mittal and helpful discussions with G. Gioia and J. Freund.

[1] Review articles on granular materials include H. M. Jaeger, S. R. Nagel, and R. P. Behringer, Rev. Mod. Phys. **68**, 1259 (1996); T. Shinbrot and F. J. Muzzio, Phys. Today **53** (3), 25 (2000).

[2] T. Boutreux, Eur. Phys. J. B **6**, 419 (1998); H. Makse, S. Havlin, P. B. King, and H. E. Stanley, Nature (London) **386**, 379 (1997).

[3] K. M. Hill, G. Gioia, and D. Amaravadi, Phys. Rev. Lett. **93**, 224301 (2004); D. V. Khakhar, A. V. Orpe, and J. M. Ottino, Powder Technol. **116**, 232 (2001).

[4] N. Jain, J. M. Ottino, and R. M. Lueptow, Phys. Rev. E **71**, 051301 (2005); N. Jain, J. M. Ottino, and R. M. Lueptow, Granular Matter **7**, 69 (2005).

[5] V. Garzó and J. Dufty, Phys. Rev. E **60**, 5706 (1999).

[6] J. E. Galvin, S. R. Dahl, and C. M. Hrenya, J. Fluid Mech. **528**, 207 (2005).

[7] M. Alam and S. Luding, Granular Matter **4**, 139 (2002).

[8] K. Feitosa and N. Menon, Phys. Rev. Lett. **88**, 198301 (2002).

[9] R. D. Wildman and D. J. Parker, Phys. Rev. Lett. **88**, 064301 (2002).

[10] The plastic beads are cellulose acetate with a standard deviation of particle diameter of 0.0508 mm (Engineering Laboratories), and the steel beads are Grade SS440C chrome steel beads with a standard deviation of particle diameter of 0.01 mm (Quackenbush).

[11] K. M. Hill, G. Gioia, and V. V. Tota, Phys. Rev. Lett. **91**, 064302 (2003).

[12] G. Gioia, S. E. Ott-Monsivais, and K. M. Hill, Phys. Rev. Lett. **96**, 138001 (2006).

[13] For fill levels of ~55%, the segregation patterns further evolve to striped segregation patterns, as in Fig. 1(j), where the concentration in the flowing layer is unsteady [3].

[14] These results are calculated considering the volume contribution of each particle to a horizontal bin of width $d/100$ centered at depth y. For example, for the volume fraction of species i in bin B centered at depth y, $\bar{f}(y)_i=\bar{f}_{i,B_y}=\Sigma_j\Sigma_{b_i}V_j^{b_i}/1024V$; the sum in j extends over all images, and the sum in b_i extends over all beads of species i in image j. Similarly, $\bar{u}(y)_i=\bar{u}_{i,B_y}=\Sigma_j\Sigma_{b_i}V_j^{b_i}u_j^{b_i}/\Sigma_j\Sigma_{b_i}V_j^{b_i}$. For more details, see [11], where the calculations are quite similar, but for monodisperse systems. Further, we subtract the drum rotation from the measured particle velocities: $\mathbf{v}=\mathbf{v}_{meas}-\omega\times\mathbf{r}$.

[15] N. Jain, J. M. Ottino, and R. M. Lueptow, Phys. Fluids **14**, 572 (2002).

[16] P. A. Cundall and O. D. Strack, Geotechnique **29**, 47 (1979).

[17] Y. Tsuji, T. Tanaka, and T. Ishida, Powder Technol. **71**, 239 (1992).

[18] N. Taberlet, P. Richard, and E. J. Hinch, Phys. Rev. E **73**, 050301(R) (2006).

[19] J. Zhang, J. B. Freund, and K. M. Hill (unpublished).

[20] The maximum volume fraction appears a bit higher for these simulations compared with the simulations and experiments where walls limit the packing.

[21] For component i, $\overline{v'v'}(y)_i=(\xi_{v,i}^2/2)\int_y^{y_b}\bar{d}(\eta)\dot{\gamma}_i^2(\eta)d\eta$ and $\overline{u'u'}(y)_i=(\xi_{u,i}^2/2)\int_y^{y_b}\bar{d}(\eta)\dot{\gamma}_i^2(\eta)d\eta$. Then we note that for mixtures, at depth η, $\bar{u}(\eta)$ and thus $\dot{\gamma}(\eta)$ are the same for both components (see Figs. 2 and 3 and associated text). Finally, for species i, $\xi_{u,i}$ and $\xi_{v,i}$ are independent of depth (see Fig. 5 and associated text). Using all this we can calculate $T_{kinem,r}=(\xi_{u,3}^2+\xi_{v,3}^2)/(\xi_{u,2}^2+\xi_{v,2}^2)$.

[22] The temperature ratio described by Feitos and Menon [8] is written in terms of $1/M_rT_r$. For our data, for $M_r=2.7$, $1/M_rT_r\approx 0.6$, and in Ref. [8], for $M_r=3$ and $M_r=3.5$, $1/M_rT_r=0.66$ and 0.69, respectively.

[23] D. V. Khakhar, J. J. McCarthy, T. Shinbrot, and J. M. Ottino, Phys. Fluids **9**, 31 (1997).

[24] S. B. Savage and C. K. K. Lun, J. Fluid Mech. **189**, 311 (1988); J. M. N. T. Gray and A. R. Thornton, Proc. R. Soc. London, Ser. A **461**, 1447 (2005).

[25] See, for example, D. M. Powell, Prog. Phys. Geogr. **22**, 1 (1998).

[26] L. Hsu, W. E. Dietrich, and L. S. Sklar, J. Geophys. Res. **113**, F02001 (2008).

[27] We define $y=0$ where the measured mixture $\bar{f}=1\%$.